Inorg. Chem. **2007**, *46*, 10354–10364

Six-Membered Ring Chelate Complexes of Ru(II): Structural and Photophysical Effects

Maria Abrahamsson,[†,§] Hans-Christian Becker,[†] Leif Hammarström,*[,†] Celine Bonnefous,[‡] Charles Chamchoumis,[‡] and Randolph P. Thummel*[,‡]

Chemical Physics, Department of Photochemistry and Molecular Science, The Ångström Laboratories, Uppsala University, Box 523, SE-751 20 Uppsala, Sweden, Department of Chemistry, University of Houston, Houston, Texas 77204-5003

Received June 17, 2007

The structural and photophysical properties of Ru(II)–polypyridyl complexes with five- and six-membered chelate rings were studied for two bis-tridentate and two tris-bidentate complexes. The photophysical effect of introducing a six-membered chelate ring is most pronounced for the tridentate complex, leading to a room-temperature excited-state lifetime of 810 ns, a substantial increase from 180 ns for the five-membered chelate ring model complex. Contrasting this, the effect is the opposite in tris-bidentate complexes, in which the lifetime decreases from 430 ns to around 1 ns in going from a five-membered to six-membered chelate ring. All of the complexes were studied spectroscopically at both 80 K and ambient temperatures, and the temperature dependence of the excited-state lifetime was investigated for both of the bis-tridentate complexes. The main reason for the long excited-state lifetime in the six-membered chelate ring bis-tridentate complex was found to be a strong retardation of the activated decay via metal-centered states, largely due to an increased ligand field splitting due to the complex having a more-octahedral geometry.

Introduction

One of the most commonly used bidentate chelating ligands is 2,2′-bipyridine (bpy), which forms five-membered chelate ring complexes with a wide range of metal ions. Because many of these complexes involve square planar or octahedral coordination, the preferred bite angle in a strain-free complex is 90°. However, the angle defined by the intersection of the orbitals containing the lone-pair electrons in the planar cisoid conformation of bpy is only 60°. Typical N−Ru−N angles for most Ru(II) complexes involving bpy are substantially greater than 60°, ranging from 75 to 80°.

In earlier work, we have modified the dihedral angle between the pyridine halves of bpy by incorporating a 3,3′-polymethylene bridge.[1] As the bridge is lengthened from one to four methylene units, the twist angle about the 2,2′ bond increases from 0 to 45°. We were somewhat surprised to discover that even the highly distorted tetramethylene-bridged ligand reacted readily with Ru(II) to form a tris complex in 56% yield. However, the spectroscopic and electronic properties of this complex were not greatly different from the parent $[Ru(bpy)_3]^{2+}$. Here, the effect of an in-plane angle distortion, as would be involved in the formation of a larger chelate ring, is investigated.

It has recently been shown that an increase in the ligand bite angle in bis-tridentate Ru(II) complexes can have significant effects on the photophysical properties.[2−4] For example, the 0.25 ns excited-state lifetime[5] of $[Ru(tpy)_2]^{2+}$ (tpy = 2,2′;6′,2″-terpyridine) was increased up to 3.0 μs, when going from five- to six-membered chelate rings, using the bqp ligand (bqp = 2,6-di(8′-quinolinyl)pyridine). The

* To whom correspondence should be addressed. E-mail: Leif@fotomol.uu.se, thummel@uh.edu.
† Uppsala University.
‡ University of Houston.
§ Present address: Department of Chemistry, Johns Hopkins University, Baltimore, MD 21218.

(1) Strekas, T. C.; Gafney, H. D.; Tysoe, S. A.; Thummel, R. P.; Lefoulon, F. *Inorg. Chem.* **1989**, *28*, 2964−2967.
(2) Abrahamsson, M.; Wolpher, H.; Johansson, O.; Larsson, J.; Kritikos, M.; Eriksson, L.; Norrby, P.-O.; Bergquist, J.; Sun, L.; Åkermark, B.; Hammarström, L. *Inorg. Chem.* **2005**, *44*, 3215−3225.
(3) Wolpher, H.; Johansson, O.; Abrahamsson, M.; Kritikos, M.; Sun, L.; Åkermark, B. *Inorg. Chem. Commun.* **2004**, *7*, 337−340.
(4) Abrahamsson, M.; Jager, M.; Osterman, T.; Eriksson, L.; Persson, P.; Becker, H. C.; Johansson, O.; Hammarstrom, L. *J. Am. Chem. Soc.* **2006**, *128*, 12616−12617.
(5) Sauvage, J.-P.; Collin, J.-P.; Chambron, J.-C.; Guillerez, S.; Coudret, C.; Balzani, V.; Barigelletti, F.; De Cola, L.; Flamigni, L. *Chem. Rev.* **1994**, *94*, 993−1019.

10.1021/ic7011827 CCC: $37.00
Published on Web 11/02/2007

Chart 1. Geometric Difference between a Bipyridine Ligand and an In-Plane Distorted Bidentate Polypyridine Ligand

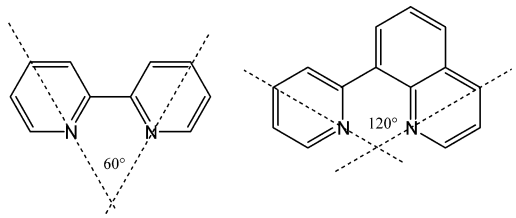

Chart 2. Ligands Included in This Study

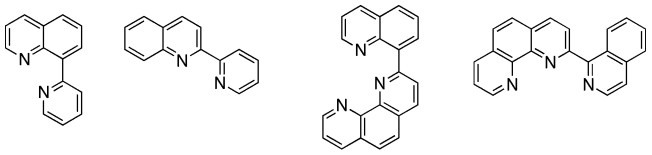

1 **2** **3** **4**

reason for this behavior is that a larger ligand bite angle leads to less interaction between the emissive ^{3}MLCT state and the nonemissive ^{3}MC state due to a destabilization of the unoccupied metal e_g orbitals, leading to less nonradiative decay of the excited state.[2−4]

The ligand 8-(pyrid-2′-yl)quinoline (**1**) is a close analogue to bpy and bears a 1,5 relationship between the two nitrogen donor atoms. The molecule has only one degree of rotational freedom and, in its planar cisoid conformation, conjugation between the two aromatic moieties is maintained. The theoretical bite angle increases to 120°, which is greater than the optimal 90°. (Chart 1.)

In this article, we will describe the preparation and Ru(II) complexation of **1** and **3**. The structural, electrochemical, and photophysical properties of these systems will be compared to isomeric systems **2** and **4**, which involve five-membered chelate rings. (Chart 2.)

Results and Discussion

Synthesis and Structure. The synthesis of ligands **1**[6] and **3**[7] as well as the preparation of the complexes[8−10] $[Ru(bpy)_2(\mathbf{2})]^{2+}$ and $[Ru(\mathbf{4})_2]^{2+}$ have been previously reported. Because of anticipated problems with steric congestion as well as stereoisomerism, we prepared only the mixed-ligand complex of **1**. This proceeded smoothly in 86% yield after a 4 h reflux in aqueous ethanol. Because of a lack of symmetry, all 26 protons of complex $[Ru(bpy)_2(\mathbf{1})]^{2+}$ were nonequivalent, and thus the ^{1}H NMR spectrum was difficult to interpret. This problem was averted by the preparation of the analogous complex using bpy-d_8 as the auxiliary ligand. The $[Ru(bpy\text{-}d_8)_2(\mathbf{1})]^{2+}$ showed only 10 resonances coming from ligand **1**, and these could be assigned in a straightforward fashion and also identified in the more-complex spectrum of the undeuterated material. Complexation of **3** required more forcing conditions, affording a 36% yield of $[Ru(\mathbf{3})_2]^{2+}$ after heating an ethylene glycol solution of the reactants in a microwave oven.

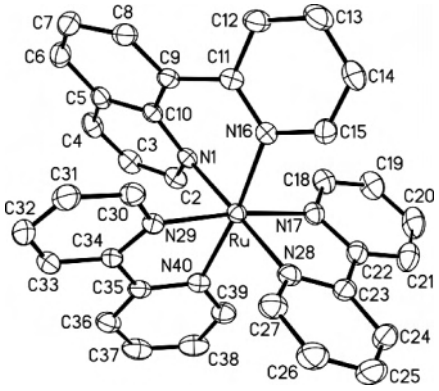

Figure 1. ORTEP plot of the cation of $[Ru(\mathbf{1})(bpy)_2](PF_6)_2$ showing atom-numbering scheme.

A characteristic feature in the ^{1}H NMR spectra of Ru(II)−polypyridine complexes is the complexation-induced shift of the proton ortho to the pyridine nitrogen, which is easily identified by its small (ca. 4.6 Hz) H−C−C−H coupling constant. In a well-organized complex, having ligands lying in mutually perpendicular planes, this proton is held over the shielding face of an orthogonal ligand and thus shifted ca. 1 ppm to a higher field. Twisting about an intraligand σ bond can lessen this effect, whereas the increased pitch of the ortho C−H bond due to six-membered ring chelation can increase the shielding.[11] In $[Ru(bpy)_2(\mathbf{1})]^{2+}$ the complexation-induced shifts for H2 and H6′ are 1.02 and 0.84 ppm, respectively, which are close to the value of 0.90 ppm for $[Ru(bpy)_3]^{2+}$, indicating that compensating effects are probably occurring.

To further characterize $[Ru(bpy)_2(\mathbf{1})]^{2+}$, a single-crystal X-ray analysis was carried out. The pertinent geometric features are summarized in Table 1 and illustrated in an ORTEP diagram of the cation shown in Figure 1. Data collecting and processing parameters are found in Table 2. The most important feature to compare are the shapes of the three chelate rings. The six-membered ring, containing N1 and N16, shows longer Ru−N bonds, especially to the quinoline moiety. The 2,2′ bond connecting quinoline and pyridine is also slightly elongated, suggesting diminished π overlap between the two halves of **1**. As expected, the N1−Ru−N16 angle has increased by almost 10°, to 88°, approaching the ideal of 90°. The other angles interior to the six-membered chelate ring are also larger, averaging about 122°, as compared to the angles interior to the five-membered chelate ring, which average around 115°. The two halves of the auxiliary bipyridine ligands are nearly coplanar with dihedral angles of 2.5 and 3.0° about the 2,2′ bond. The ligand **1**, on the other hand, shows a substantial twist about the 2,2′ bond with a dihedral angle of about 34°, which is consistent with the torsion angle that has been observed in a related six-membered chelate ring[12] and in complex

(6) Delis, J. G. P.; Rep, M.; Rulke, R. E.; vanLeeuwen, P.; Vrieze, K.; Fraanje, J.; Goubitz, K. *Inorg. Chim. Acta* **1996**, *250*, 87−103.
(7) Hu, Y.-Z.; Wilson, M. H.; Zong, R.; Bonnefous, C.; McMillin, D. R.; Thummel, R. P. *Dalton Trans.* **2005**, 354−358.
(8) Jahng, Y.; Thummel, R. P.; Bott, S. G. *Inorg. Chem.* **1997**, *36*, 3133−3138.
(9) Anderson, S.; Seddon, K. R.; Wright, R. D.; Cocks, A. T. *Chem. Phys. Lett.* **1980**, *71*, 220−223.
(10) Thummel, R. P.; Decloitre, Y. *Inorg. Chim. Acta* **1987**, *128*, 245−249.
(11) Downard, A. J.; Honey, G. E.; Steel, P. J. *Inorg. Chem.* **1991**, *30*, 3733−3737.

Table 1. Selected Geometric Properties for $[Ru(\mathbf{1})(bpy)_2](PF_6)_2$ from X-ray Crystallography.

	N1, N16 Ring		N17, N28 Ring		N29, N40 Ring	
Bond Lengths (Å)	Ru−N1	2.114(3)	Ru−N17	2.060(3)	Ru−N29	2.060(3)
	Ru−N16	2.079(3)	Ru−N28	2.049(3)	Ru−N40	2.066(3)
	C9−C11	1.489(5)	C22−C23	1.473(5)	C34−C35	1.478(5)
Bond Angles (deg)	N1−Ru−N16	88.05(10)	N17−Ru−N28	78.94(11)	N29−Ru−N40	78.51(11)
	C10−N1−Ru	118.9(2)	C22−N17−Ru	115.3(2)	C34−N29−Ru	114.5(2)
	C9−C10−N1	121.0(3)	C23−C22−N17	114.7(3)	C35−C34−N29	114.6(3)
	C11−C9−C10	124.6(3)	N28−C23−C22	114.6(3)	N40−C35−C34	114.6(3)
	N16−C11−C9	121.9(3)	Ru−N28−C23	116.0(20	Ru−N40−C35	113.9(2)
	Ru−N16−C11	122.8(2)				
Dihedral Angles (deg)	C8−C9−C11−C12	−30.6(4)	C21−C22−C23−C24	−2.6(6)	C33−C34−C35−C36	3.5(5)
	C10−C9−C11−N16	−36.9(5)	N17−C22−C23−N28	−2.5(4)	N29−C34−C35−C40	2.5(4)
	C9−C10−N1−Ru	32.6(4)				
	N1−C10−C9−C11	14.6(5)				
	C9−C11−N16−Ru	5.3(4)				

Table 2. Data Collection and Processing Parameters for $[Ru(\mathbf{1})(bpy)_2](PF_6)_2-CH_3CN$.

empirical formula	$C_{36}H_{29}N_7F_{12}P_2Ru$	
fw	950.67	
T (K)	223(2)	
wavelength (Å)	0.71073	
cryst syst	monoclinic	
space group	$P2(1)/c$	
unit cell dimensions	$a = 20.3944(12)$ Å	$\alpha = 90°$
	$b = 12.7894(8)$ Å	$\beta = 109.088(1)°$
	$c = 15.2668(9)$ Å	$\gamma = 90°$
V(Å^3)	3763.1(4)	
Z	4	
D_{calcd} (Mg/m^3)	1.678	
absorption coefficient (mm^{-1})	0.600	
cryst size (mm^3)	0.50 × 0.24 × 0.20	
θ range for data collection (deg)	1.91−23.28	
reflns collected	16 561	
independent reflns	5602 [R(int) = 0.0193]	
max. and min. transmission	0.8580 and 0.7359	
refinement method	Full-matrix least-squares on F^2	
data/restraints/params	5379/0/519	
GOF on F^2	1.047	
Final R indices [$I > 4\sigma(I)$]	R1 = 0.0333, wR2 = 0.0887	
R indices (all data)	R1 = 0.0388, wR2 = 0.0952	

$[Ru(bqp)_2]^{2+}$, which has only six-membered chelate rings.[4] The other dihedral angles interior to the six-membered chelate ring also evidence a substantial amount of nonplanarity.

DFT Calculations. Geometries of $[Ru(\mathbf{3})_2]^{2+}$ and $[Ru(\mathbf{4})_2]^{2+}$ were optimized at the B3LYP/LANL2DZ level of theory using the *Gaussian 03* program suite.[13] Solvent effects were not taken into account. DFT calculations with this basis set have been shown to produce good results at a reasonable computational cost.[14] The optimized structures are remarkably different: in $[Ru(\mathbf{3})_2]^{2+}$, the bite angle is close to 180°, and the quinoline moiety is twisted 27° out of the phenanthroline plane. This geometry is similar to the bite angle and nonplanarity of the aromatic rings in the complex $[Ru(bqp)_2]^{2+}$.[4] In contrast, the bite angle in $[Ru(\mathbf{4})_2]^{2+}$ is calculated to be 157°, whereas the angle between the aromatic rings is only 8°. Even though the geometry optimizations were carried out at a relatively low level of sophistication, the predicted difference between $[Ru(\mathbf{3})_2]^{2+}$ and $[Ru(\mathbf{4})_2]^{2+}$ is significant enough to warrant consideration in the analysis of the photophysical characteristics.

The predicted geometries are borne out in the electronic absorption spectra calculated using time-dependent DFT at the B3LYP/LANL2DZ level. The first singlet−singlet excitation, being a metal-to-ligand charge-transfer (MLCT) transition in the red part of the visible absorption band for both complexes, is calculated to occur at 18 000 cm^{-1} for $[Ru(\mathbf{3})_2]^{2+}$ and at 17 200 cm^{-1} for $[Ru(\mathbf{4})_2]^{2+}$. The fact that the calculated transitions follow the experimental absorption spectra suggests that the calculated geometries are qualitatively correct. The resulting frontier orbitals are shown in the Supporting Information (Figure S1). The HOMO of $[Ru(\mathbf{3})_2]^{2+}$ and $[Ru(\mathbf{4})_2]^{2+}$ is essentially metal-based, as is typical for Ru(II)−polypyridine complexes, whereas the

(12) Bardwell, D. A.; Jeffery, J. C.; Schatz, E.; Tilley, E. E. M.; Ward, M. D. *J. Chem. Soc., Dalton Trans.* **1995**, 825−834.

(13) Frisch, M. J.; Trucks, G. W.; Schlegel, H. B.; Scuseria, G. E.; Robb, M. A.; Cheeseman, J. R.; Montgomery, J. A., Jr.; Vreven, T.; Kudin, K. N.; Burant, J. C.; Millam, J. M.; Iyengar, S. S.; Tomasi, J.; Barone, V.; Mennucci, B.; Cossi, M.; Scalmani, G.; Rega, N.; Petersson, G. A.; Nakatsuji, H.; Hada, M.; Ehara, M.; Toyota, K.; Fukuda, R.; Hasegawa, J.; Ishida, M.; Nakajima, T.; Honda, Y.; Kitao, O.; Nakai, H.; Klene, M.; Li, X.; Knox, J. E.; Hratchian, H. P.; Cross, J. B.; Bakken, V.; Adamo, C.; Jaramillo, J.; Gomperts, R.; Stratmann, R. E.; Yazyev, O.; Austin, A. J.; Cammi, R.; Pomelli, C.; Ochterski, J. W.; Ayala, P. Y.; Morokuma, K.; Voth, G. A.; Salvador, P.; Dannenberg, J. J.; Zakrzewski, V. G.; Dapprich, S.; Daniels, A. D.; Strain, M. C.; Farkas, O.; Malick, D. K.; Rabuck, A. D.; Raghavachari, K.; Foresman, J. B.; Ortiz, J. V.; Cui, Q.; Baboul, A. G.; Clifford, S.; Cioslowski, J.; Stefanov, B. B.; Liu, G.; Liashenko, A.; Piskorz, P.; Komaromi, I.; Martin, R. L.; Fox, D. J.; Keith, T.; Al-Laham, M. A.; Peng, C. Y.; Nanayakkara, A.; Challacombe, M.; Gill, P. M. W.; Johnson, B.; Chen, W.; Wong, M. W.; Gonzalez, C.; Pople, J. A. *Gaussian 03*, revision B.05; Gaussian, Inc.: Wallingford, CT, 2003.

(14) Gorelsky, S. I.; Lever, A. B. P. *J. Organomet. Chem.* **2001**, *635*, 187−196.

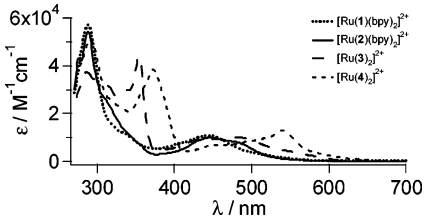

Figure 2. UV−vis electronic spectrum in CH_3CN.

Table 3. UV−Vis and Electrochemical Data, Recorded in Ch_3CN and Reported Versus $Fc^{+/0}$ as Internal Standard[a]

complex	λ_{max}/nm ($\epsilon\times10^{-4}$ /$M^{-1}cm^{-1}$)	$E_{1/2}$/V $Ru^{2+/+}$	$Ru^{3+/2}$
$[Ru(\mathbf{1})(bpy)_2]^{2+}$	288 (5.7), 339sh (1.1), 445 (1.1)	−1.61	0.84
$[Ru(\mathbf{2})(bpy)_2]^{2+}$	288 (5.4), 310sh (2.6), 445 (1.0)	−1.49	0.93
$[Ru(\mathbf{3})_2]^{2+}$	287 (3.7), 354 (4.4), 485 (1.0)	−1.49	0.78
$[Ru(\mathbf{4})_2]^{2+}$	290 (5.1), 372 (3.9), 540 (1.3)	−1.24	0.91
$[Ru(bpy)_3]^{2+}$ [b]	288 (7.9), 450 (1.4)	−1.74	0.88
$[Ru(tpy)_2]^{2+}$ [c]	272 (3.8), 308(6.4), 476 (1.8)	−1.62	0.92

[a] Reference complexes included for comparison. [b] From ref 4. [c] Absorption data from Anderson *et. al. Inorg. Chem.* **1995**, *34*, 6145, and electrochemistry data from ref 5.

LUMO is ligand-based. The LUMO extends over both ligand fragments, in spite of the twist in $[Ru(\mathbf{3})_2]^{2+}$. In $[Ru(\mathbf{4})_2]^{2+}$, the LUMO has a higher density on the three central rings. The local LUMO symmetry of the five- and six-chelate rings is the same, meaning that the sign on all of the coordinating nitrogens is the same in both complexes.

Electronic Absorption Spectra. Electronic absorption spectra of the complexes are shown in Figure 2. The wavelengths of the absorption maxima and the values of the molar absorption coefficients for all of the complexes are listed in Table 3. In the visible region, the absorption is dominated by the expected ^{1}MLCT transitions between 400 and 600 nm for all of the complexes.[5,15] It is noteworthy that the MLCT band is strongly red-shifted in $[Ru(\mathbf{4})_2]^{2+}$, as compared to the other complexes. The extinction coefficients of these bands are approximately 1×10^4 M^{-1} cm^{-1}, which is typical for Ru(II)−polypyridine complexes. The UV region for $[Ru(bpy)_2(\mathbf{1})]^{2+}$ and $[Ru(bpy)_2(\mathbf{2})]^{2+}$ is dominated by ligand-centered transitions, where the bpy transition at 288 nm is dominant, whereas $[Ru(\mathbf{3})_2]^{2+}$ and $[Ru(\mathbf{4})_2]^{2+}$ show an additional strong band at about 350 and 380 nm, respectively. These bands can be attributed either to higher-energy MLCT transitions or to ligand-centered (LC) transitions,[5,15] but as they are rather narrow and intense we believe they are LC transition bands.

Weaker bands in this region were observed for the free ligands, but complexation changes the ligand geometry to a large extent, in particular for ligand **3**. Although $[Ru(\mathbf{3})_2]^{2+}$ and $[Ru(\mathbf{4})_2]^{2+}$ contain the same structural units, phenanthroline and quinoline, the absorption spectra clearly show that their electronic properties are different.

Electrochemical Properties. The electrochemical properties of the complexes were investigated by cyclic voltammetry in acetonitrile, and the results are summarized in Table 3. The reversible metal-based one-electron oxidations fall in the range 0.78−0.93 V versus Fc^+/Fc. The first ligand-based reductions are found in the range −1.24 to −1.61 V and are quasi-reversible for all of the complexes. Under the same conditions, $[Ru(bpy)_3]^{2+}$ displays a metal-based oxidation at 0.88 V, and its first reduction is at −1.74 V, whereas the corresponding results for $[Ru(tpy)_2]^{2+}$ are 0.92 and −1.62 V, respectively.[2,5] For $[Ru(bpy)_2(\mathbf{1})]^{2+}$ and $[Ru(bpy)_2(\mathbf{2})]^{2+}$, three ligand-based reductions can be observed in the potential region investigated. In $[Ru(bpy)_2(\mathbf{2})]^{2+}$, the first reduction occurs at 0.25 V lower potential than that in $[Ru(bpy)_3]^{2+}$, so that it can be assigned to the reduction of ligand **2**, in analogy to $[Ru(bpy)_2(biq)]^{2+}$ (biq = biquinoline).[16] For $[Ru(bpy)_2(\mathbf{1})]^{2+}$, the first reduction involves ligand **1** because it occurs at 0.1 V lower potential than in $[Ru(bpy)_3]^{2+}$, whereas the second reduction is almost the same for both complexes. For the homoleptic complexes $[Ru(\mathbf{3})_2]^{2+}$ and $[Ru(\mathbf{4})_2]^{2+}$, two irreversible ligand-based reductions are observed, for the successive one-electron reduction of the two ligands. The less-negative potential for ligand reduction compared to $[Ru(tpy)_2]^{2+}$ explains the red-shifted MLCT absorption bands above, as the MLCT energy typically shows linear dependence on the difference in potential between the first oxidation and reduction ($\Delta E_{1/2}$).[15] A quantitative comparison of $\Delta E_{1/2}$ and the excited-state energy estimated from emission data support a ^{3}MLCT assignment of the lowest excited-state in $[Ru(\mathbf{3})_2]^{2+}$ and $[Ru(\mathbf{4})_2]^{2+}$ (below).

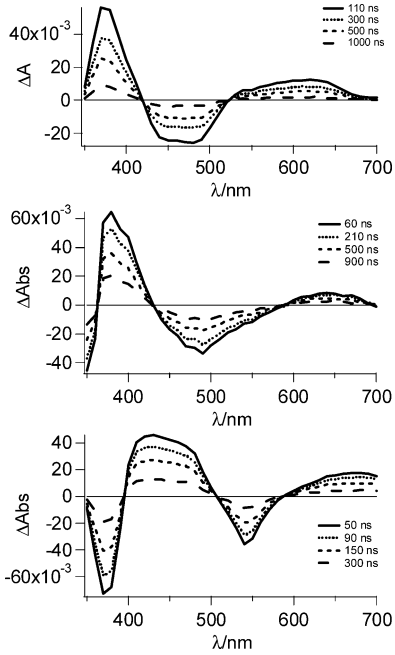

Figure 3. Nanosecond transient absorption spectra in deoxygenated acetonitrile. Upper panel: $[Ru(bpy)_2(\mathbf{2})]^{2+}$, middle panel: $[Ru(\mathbf{3})_2]^{2+}$, lower panel: $[Ru(\mathbf{4})_2]^{2+}$.

Transient Absorption Spectroscopy. Nanosecond transient absorption spectra recorded after laser flash excitation of $[Ru(bpy)_2(\mathbf{2})]^{2+}$, $[Ru(\mathbf{3})_2]^{2+}$, and $[Ru(\mathbf{4})_2]^{2+}$ in deoxygenated acetonitrile are shown in Figure 3. The lifetime of $[Ru(bpy)_2(\mathbf{1})]^{2+}$ was too short to allow analysis by this technique. Attempts to measure the transient absorption on the femtosecond time scale failed because of sample

(15) Juris, A.; Balzani, V.; Barigelletti, F.; Campagna, S.; Belser, P.; Von, Zelewsky, A. *Coord. Chem. Rev.* **1988**, *84*, 85−277.

(16) Barigelletti, F.; Juris, A.; Balzani, V.; Belser, P.; Von, Zelewsky, A. *Inorg. Chem.* **1987**, *26*, 4115−4119.

Table 4. Emission Properties of the Complexes in Deoxygenated MeOH/EtOH

	298 K					80 K				
complex	λ_{max} (nm)	$\Phi \times 10^{-3}$	τ (ns)	$k_r{}^a$ (s^{-1})	$k_{nr}{}^a$ (s^{-1})	λ_{max} (nm)	Φ	τ (μs)	$k_r{}^a$ (s^{-1})	$k_{nr}{}^a$ (s^{-1})
$[Ru(\mathbf{1})(bpy)_2]^{2+}$	707	0.4	~1			656	0.05	8.2; 1.3		
$[Ru(\mathbf{2})(bpy)_2]^{2+}$	705	9	430	2.1×10^4	2.3×10^6	659	0.15	2.3	6.6×10^4	3.7×10^5
$[Ru(\mathbf{3})_2]^{2+}$	712	5	810	6.2×10^3	1.2×10^6	672	0.05	4.1	1.2×10^4	2.3×10^5
$[Ru(\mathbf{4})_2]^{2+}$	762	2	180	1.1×10^4	5.5×10^6	721	0.05	1.2	3.8×10^4	8.0×10^5
$[Ru(bpy)_3]^{2+}$ [b]	630	89	1150	7×10^4	8×10^5	582	0.33	5.1	6×10^4	1×10^5
$[Ru(tpy)_2]^{2+}$ [c]			0.25			598	0.48	11.0	4×10^4	5×10^4

[a] Radiative and nonradiative rate constants are calculated from the quantum yields and excited-state lifetimes given in the table. [b] From ref 4. [c] From ref 5.

decomposition. The nanosecond transient absorption spectra all display a uniform excited-state decay constant over the whole spectral range that is equal to the value obtained from the emission decay, (Table 4). For $[Ru(bpy)_2(\mathbf{2})]^{2+}$, the excited-state absorption spectrum is very similar to that for $[Ru(bpy)_3]^{2+}$.[17,18] Because ligand **2** was the first to be reduced electrochemically, we assign the lowest excited state to the formal $[Ru(III)(bpy)_2(\mathbf{2}^{\bullet-})]^{2+}$ MLCT state. In analogy with $[Ru(bpy)_3]^{2+}$, the absorption below 400 nm can then be attributed to ligand-centered $\mathbf{2}^{\bullet-}$ transitions.[17,18] A significant excited-state absorption above 530 nm is also seen, and again in analogy with the case of $[Ru(bpy)_3]^{2+}$, we attribute this to LC and ligand-to-metal centered transitions. The other two complexes display the same qualitative features, although shifted to the red so that also the ligand-centered ground state bleach is seen in the near UV region. The relatively strong excited-state absorption for $[Ru(\mathbf{4})_2]^{2+}$ could possibly indicate that the initially formed ^{3}MLCT state establishes an equilibrium with a ligand centered excited state. However, femtosecond transient absorption measurements on $[Ru(\mathbf{4})_2]^{2+}$ (not shown) show that all of the bands are formed with the same pulse width-limited rate. Also, the proposed LC absorption of $[Ru(III)(\mathbf{4})(\mathbf{4}^{\bullet-})]^{2+}$ around 450 nm presumably extends further in the UV, but the net transient absorption is cut by the strong ground-state bleach. In conclusion, all three complexes show transient absorption spectra on the nanosecond time scale that, based on the similarity to other Ru(II)−polypyridine complexes, can be attributed to the lowest excited ^{3}MLCT state.

Emission Spectroscopy. The complexes show emission behavior typical of the ^{3}MLCT state, and the emission properties are summarized in Table 4. The excited-state energies (E_{em}), as estimated from the 0−0 transition at 80 K,[19−21] are lower than those for the parent $[Ru(bpy)_3]^{2+}$, although the decrease is not very dramatic for $[Ru(bpy)_2(\mathbf{1})]^{2+}$, $[Ru(bpy)_2(\mathbf{2})]^{2+}$, and $[Ru(\mathbf{3})_2]^{2+}$. For $[Ru(\mathbf{4})_2]^{2+}$, however, the excited-state energy is much lower. Also, the room-temperature emission of the latter is very red-shifted compared to the other complexes. The dependence of E_{em} on $\Delta E_{1/2}$ for Ru(II)−polypyridine complexes

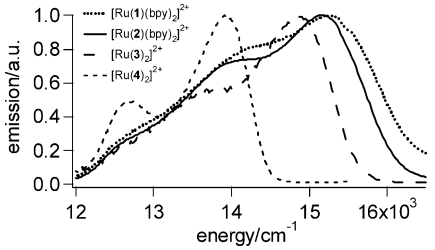

Figure 4. Emission spectra in MeOH:EtOH (1:4 by volume) at 80 K.

with a lowest state of ^{3}MLCT character is typically linear, with a slope somewhat less than unity (in units of *e*).[15] This relation is also observed in the series $[Ru(tpy)_2]^{2+}$, $[Ru(\mathbf{3})_2]^{2+}$, and $[Ru(\mathbf{4})_2]^{2+}$ for which $\Delta E_{1/2} = 2.54$, 2.27, and 2.15 V, respectively, whereas $E_{em} = 2.07$, 1.85, and 1.72 eV. This supports the assignment of a lowest excited state of the ^{3}MLCT type.

An analysis of the low-temperature emission spectral shape (Figure 4) can provide information about factors that govern nonradiative decay of the ^{3}MLCT state such as vibrational modes that are coupled to the transitions and geometric differences between the ground- and excited-state structures. Following the approach of Meyer and co-workers,[19−21] the low-temperature emission spectra were fitted to a series of Gaussians according to eq 1.

$$I(E) = \sum_{n_M}\sum_{n_L}\left(\frac{E_{00} - n_M\bar{\nu}_M - n_L\bar{\nu}_L}{E_{00}}\right)^4\left(\frac{S_M{}^{n_M}}{n_M!}\right)\left(\frac{S_L{}^{n_L}}{n_L!}\right)\times \left\{\exp\left(-4\log 2\left(\frac{E - E_{00} + n_M\bar{\nu}_M + n_L\bar{\nu}_L}{\bar{\nu}_{1/2}}\right)^2\right)\right\} \quad (1)$$

In this expression, E_{00} is the wave number of the 0−0 electronic transition, ν_M and ν_L are the wave numbers of the relevant medium and low-frequency vibrational transitions, respectively, n_M and n_L are the corresponding vibrational state quantum numbers, and $\nu_{1/2}$ is the full width at half-maximum of the Gaussians. S_M and S_L are the Huang−Rhys factors quantifying the nuclear distortion between the ground and excited states as $S_i = \lambda_i/\nu_i$, where λ_i and ν_i are the reorganization energy and vibrational quantum, respectively, for the relevant vibrational coordinate. It is assumed that one medium (m) and one low (l) frequency vibrational modes are sufficient to reproduce the experimentally obtained data. The results from the analysis are summarized in Table 5. Typically, the distortion S_i is smaller when the excess electron density can be delocalized over a larger ligand, leading to a

(17) Sun, H.; Hoffman, M. Z. *J. Phys. Chem.* **1993**, *97*, 11956−11959.
(18) McCusker, J. K. *Acc. Chem. Res.* **2003**, *36*, 876−887.
(19) Caspar, J. V.; Meyer, T. J. *Inorg. Chem.* **1983**, *22*, 2444−2453.
(20) Treadway, J. A.; Loeb, B.; Lopez, R.; Anderson, P. A.; Keene, F. R.; Meyer, T. J. *Inorg. Chem.* **1996**, *35*, 2242−2246.
(21) Hammarström, L.; Barigelletti, F.; Flamigni, L.; Indelli, M. T.; Armaroli, N.; Calogero, G.; Guardigli, M.; Sour, A.; Collin, J.-P.; Sauvage, J.-P. *J. Phys. Chem. A* **1997**, *101*, 9061−9069.

Table 5. Spectral Fit Parameters from the 80 K Steady-State Emission Experiments

complex	E_{00} (cm^{-1})	ν_M[a] (cm^{-1})	S_M	ν_L [a] (cm^{-1})	S_L	$\nu_{1/2}$ (cm^{-1})
$[Ru(\mathbf{1})(bpy)_2]^{2+}$	15 540	1350	0.91	400	0.83	1230
$[Ru(\mathbf{2})(bpy)_2]^{2+}$	15 370	1350	0.83	400	0.59	1040
$[Ru(\mathbf{3})_2]^{2+}$	15 060	1350	0.68	400	1.02	770
$[Ru(\mathbf{4})_2]^{2+}$	13 860	1350	0.57	400	0.35	720

[a] Locked to a value typical for Ru(II)−polypyridines, see refs 19−21.

lower relative intensity of the second vibronic peak.[22] Thus, whereas S_M is about 0.95 for $[Ru(bpy)_3]^{2+}$ it is about 0.5 for $[Ru(ttpy)_2]^{2+}$ (ttpy = 4′-toluylterpyridine).[21] In the present case, S_M is 0.57−0.68 for the tridentate complexes, whereas it is larger for the bidentate ones. The spectra of the latter also show much less structure, which is reflected in larger distortion along the low-frequency Ru−N modes (S_L) and the Gaussian half-widths, in particular for $[Ru(bpy)_2(\mathbf{1})]^{2+}$. This distortion is presumably due to a steric interaction between the ligands, due to the presence of the quinoline subunit. This has been observed in other $[Ru(bpy)_2(N{-}N)]^{2+}$ complexes where N−N is a six-substituted bpy or biquinoline.[23,24] These complexes also show a less-resolved low-temperature emission structure as compared to unsubstituted $[Ru(bpy)_3]^{2+}$.[24]

The emission lifetimes for all four complexes are a few microseconds at 80 K (Table 4), which is typical for Ru(II)-polypyridines. For $[Ru(\mathbf{1})(bpy)_2]^{2+}$, the decay is biexponential. At room temperature, the lifetimes obtained from time-resolved emission and transient absorption are the same, so the emission decay can safely be assumed to monitor the decay of the lowest excited state (^{3}MLCT). $[Ru(bpy)_2(\mathbf{1})]^{2+}$ exhibits a main component at room-temperature that is very short-lived, around 1 ns, whereas $[Ru(bpy)_2(\mathbf{2})]^{2+}$ has a lifetime of 430 ns. The value for $[Ru(bpy)_2(\mathbf{1})]^{2+}$ is significantly shorter than that for the parent complex $[Ru(bpy)_3]^{2+}$, showing that a six-membered chelate ring does not necessarily increase the excited-state lifetime in tris-bidentate ruthenium(II) complexes. For the bis-tridentate complexes, however, both complexes show substantially increased excited-state lifetimes as compared to the 250 ps of the parent tridentate complex $[Ru(tpy)_2]^{2+}$ (810 ns for $[Ru(\mathbf{3})_2]^{2+}$ and 180 ns for $[Ru(\mathbf{4})_2]^{2+}$). This increase in excited-state lifetime can possibly be explained by the lower excited-state energy relative to that of $[Ru(tpy)_2]^{2+}$. A lower excited-state energy slows down the activated nonradiative decay via metal-centered (MC) states, but on the other hand, the energy gap law[25−29] predicts that the amount of nonradiative decay directly to the ground state should also increase as the excited-state energy is lowered (Scheme 1). Furthermore, the six-membered chelate rings in $[Ru(\mathbf{3})_2]^{2+}$ provide a more-octahedral complex and thus a stronger ligand field that reduces deactivation via MC states.

Scheme 1. Excited-State Manifold for Ru(II)−Polypyridine Complexes

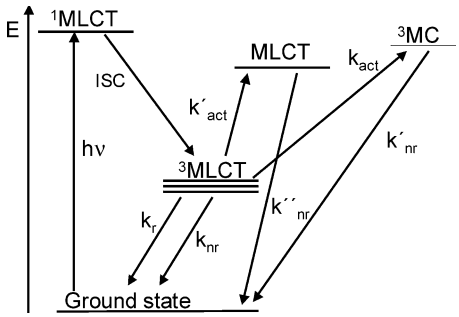

To disentangle the different contributions to the excited-state deactivation and thus understand the reason for the 1000-fold increase in lifetime compared to $[Ru(tpy)_2]^{2+}$, the temperature dependence of the emission lifetime of the two bis-tridentate complexes was investigated (below).

The radiative and nonradiative decay rate constants were calculated from the emission lifetimes and the quantum yields at low temperature, just above the glass-fluid transition (150 K) and ambient temperature. The radiative rate constants are, as expected, almost unaffected in going from 80 to 150 K, whereas they, unexpectedly, seem to decrease at higher temperatures. The nonradiative rate constants vary, as expected, with temperature. Typically, the radiative rate constants for Ru(II)−polypyridyl complexes are in the range 10^4-10^5 s^{-1}, but $[Ru(\mathbf{3})_2]^{2+}$ and $[Ru(\mathbf{4})_2]^{2+}$ exhibit somewhat lower values. It should be noted that although the low quantum yields for emission at room temperature are all in the same range as those reported for numerous Ru(II)−polypyridyl complexes, at 80 K, all of the complexes have emission quantum yields substantially lower than $[Ru(bpy)_3]^{2+}$ and $[Ru(tpy)_2]^{2+}$, which have $\Phi = 0.33$ and 0.48, respectively.[15,30]

Temperature Dependence of the Emission Lifetime. From temperature-dependent measurements of emission lifetimes and quantum yields, a model for ^{3}MLCT deactivation in $[Ru(bpy)_3]^{2+}$ and related complexes has emerged (Scheme 1).[15,31,32] The lowest-energy ^{3}MLCT state is composed of at least three closely lying ^{3}MLCT states (ΔE = 60 cm^{-1}), which kinetically behave as one at $T > 77$ K. This quasistate can decay directly to the ground state radiatively (k_r) or nonradiatively (k_{nr}). There is also an activated decay channel, which occurs via the population (k_{act}) of short-lived ^{3}MC states. This pathway dominates the room-temperature deactivation of $[Ru(tpy)_2]^{2+}$. In addition, there is at least one more MLCT state accessible at ambient temperature that is more short-lived. In complexes where deactivation via MC states is less pronounced, the involve-

(22) Coe, B. J.; Thompson, D. W.; Culbertson, C. T.; Schoonover, J. R.; Meyer, T. J. *Inorg. Chem.* **1995**, *34*, 3385−3395.
(23) Hammarstrom, L.; Alsins, J.; Borje, A.; Norrby, T.; Zhang, L. A.; Akermark, B. *J. Photochem. Photobiol. A* **1997**, *102*, 139−150.
(24) Barigelletti, F.; Belser, P.; Von, Zelewsky, A.; Juris, A.; Balzani, V. *J. Phys. Chem.* **1985**, *89*, 3680−3684.
(25) Caspar, J. V.; Kober, E. M.; Sullivan, P.; Meyer, T. J. *J. Am. Chem. Soc.* **1982**, *104*, 630−632.
(26) Englman, R.; Jortner, J. *J. Mol. Phys.* **1970**, *18*, 145.
(27) Kober, E. M.; Caspar, J. V.; Lumpkin, R. S.; Meyer, T. J. *J. Phys. Chem.* **1986**, *90*, 3722−3734.
(28) Caspar, J. V.; Meyer, T. J. *J. Phys. Chem.* **1983**, *87*, 952−957.
(29) Caspar, J. V.; Sullivan, B. P.; Kober, E. M.; Meyer, T. J. *Chem. Phys. Lett.* **1982**, *91*, 91−95.
(30) Stone, M. L.; Crosby, G. A. *Chem. Phys. Lett.* **1981**, *79*, 169−173.
(31) Meyer, T. J. *Pure Appl. Chem.* **1986**, *58*, 1193−1206.
(32) Crosby, G. A. *Acc. Chem. Res.* **1975**, *8*, 231−238.

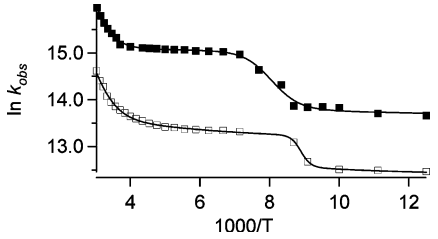

Figure 5. Temperature dependence of the observed emission decay rate constant. Markers are experimental data and solid lines are fits according to eq 2. Open squares: $[Ru(\mathbf{3})_2]^{2+}$, filled squares: $[Ru(\mathbf{4})_2]^{2+}$.

ment of this so-called fourth MLCT state can be observed as an activated process in the temperature-dependent data.[16,33−38] It should be pointed out that the details of this model have been deduced from data for Ru−bipyridine and Ru−terpyridine type complexes and that additional states may be relevant for other types of chromophoric ligands.

The temperature dependence of the emission lifetime for $[Ru(\mathbf{3})_2]^{2+}$ and $[Ru(\mathbf{4})_2]^{2+}$ was determined in the region 80−330 K. The data was fitted to eq 2[15] as shown in Figure 5.

$$k_{obs} = k_0 + \frac{M}{1 + e^{C(1/T - 1/T_m)}} + A_1 e^{-\Delta E_1/RT} + A_2 e^{-\Delta E_2/RT} \quad (2)$$

In this equation, $k_0 = k_r + k_{nr(0)}$ at 80 K, where k_r is usually assumed to be temperature independent at $T > 77$ K, and the temperature dependence of k_{nr} is described by the other terms. The second, empirical term describes the increase of k_{nr} as the solvent glass melts. The first Arrhenius term describes a weak temperature dependence of k_{nr} attributed to thermal redistribution between the three closely spaced ^{3}MLCT states, for which the higher of them has larger values of k_{nr}. The second Arrhenius term describes activated decay via population of higher-lying excited states, typically MC states.

The parameters obtained from the fit to eq 2 are found in Table 6. The first two temperature-dependent terms are unremarkable and will be discussed no further, suffice to say that the apparent variation in T_m will mainly affect the first Arrhenius term. For the parent tridentate complex, $[Ru(tpy)_2]^{2+}$ deactivation via MC states represents more than 95% of the MCLT decay at room temperature. This is reflected in a high frequency factor $A_2 = 1.9 \times 10^{13}$ s^{-1} and a relatively low activation energy for crossing to the MC state, $\Delta E_2 = 1500$ cm^{-1}, giving an observed lifetime at room temperature of only 250 ps.[5] For comparison, in $[Ru(bpy)_3]^{2+}$ the room-temperature lifetime is 950 ns and $\Delta E_2 = 4000$ cm^{-1}.[15]

For the complexes studied here, $[Ru(\mathbf{3})_2]^{2+}$ and $[Ru(\mathbf{4})_2]^{2+}$, the frequency factor A_2 is much lower, and the activation energy ΔE_2 is higher than that for $[Ru(tpy)_2]^{2+}$. As a consequence, this term contributes to only about one-half of the total room-temperature decay in both complexes. Thus, the main reason for the much longer lifetime for these complexes (810 and 180 ns for $[Ru(\mathbf{3})_2]^{2+}$ and $[Ru(\mathbf{4})_2]^{2+}$, respectively) as compared to the parent complex $[Ru(tpy)_2]^{2+}$ is that deactivation via MC states is slowed down by at least three orders of magnitude.

This conclusion raises several questions regarding the possible deactivation pathways: (i) is deactivation via MC states slowed down because the MC energy is raised, or because the MLCT energy is lowered, and if the former is true, is this a result of the introduction of a six-membered chelate ring; (ii) to what extent is the rate of direct deactivation to the ground state (k_{nr}) affected by the lowering of the MLCT energy; (iii) does the activated process observed at higher temperatures, corresponding to the last term of eq 2, involve an MC state or a higher-energy MLCT state. The following section will address these questions and discuss the results in the tris-bidentate complexes.

Discussion of the Deactivation Pathways. (i) Deactivation via MC States. The are only a few bis-tridentate complexes where the different decay pathways have been analyzed by temperature-dependent emission measurements, which limits detailed comparisons. Nevertheless, it is clear that ruthenium complexes that have an emission energy similar to $[Ru(\mathbf{3})_2]^{2+}$ typically do not reach a room-temperature lifetime of 810 ns.[39−42] This hold for complexes with simple electron-donating and -accepting groups or with cyclometalating or nitrogen-based anionic ligands. Only in binuclear complexes with strongly delocalized MLCT states have lifetimes of several hundred nanoseconds been reached due to a combination of effects such as a smaller geometric distortion of the MLCT state.[21,43] Note that the long-lived emission reported for complexes with a coupled organic triplet does not represent a long ^{3}MLCT lifetime, only a low fractional ^{3}MLCT population (analogous to delayed fluorescence). From these comparisons, it is clear that the long MLCT lifetime observed for $[Ru(\mathbf{3})_2]^{2+}$ cannot be explained just by a lowering the MLCT energy. Instead, we have recently shown examples where the activation energy for ^{3}MLCT−^{3}MC surface crossing increases for bis-tridentate complexes with six-membered chelate rings and ascribed it to the better octahedral coordination geometry caused by the larger bite angle.[2,4] This is a possible explanation for the slower deactivation rate through the ^{3}MC channel also in the case of $[Ru(\mathbf{3})_2]^{2+}$. In contrast, the slow deactivation via ^{3}MC states in $[Ru(\mathbf{4})_2]^{2+}$ must have a different explanation, as this should have a geometry similar to that of $[Ru(tpy)_2]^{2+}$. It can instead be attributed to its much-lower ^{3}MLCT energy,

(33) Allen, G. H.; White, R. P.; Rillema, D. P.; Meyer, T. J. *J. Am. Chem. Soc.* **1984**, *106*, 2613−2620.
(34) Rillema, D. P.; Allen, G.; Meyer, T. J.; Conrad, D. *Inorg. Chem.* **1983**, *22*, 1617−1622.
(35) Barigelletti, F.; Juris, A.; Balzani, V.; Belser, P.; Von, Zelewsky, A. *Inorg. Chem.* **1983**, *22*, 3335−3339.
(36) Barigelletti, F.; Juris, A.; Balzani, V.; Belser, P.; Von, Zelewsky, A. *J. Phys. Chem.* **1987**, *91*, 1095−1098.
(37) Benniston, A. C.; Chapman, G.; Harriman, A.; Mehrabi, M.; Sams, C. A. *Inorg. Chem.* **2004**, *43*, 4227−4233.
(38) Amini, A.; Harriman, A.; Mayeux, A. *Phys. Chem. Chem. Phys.* **2004**, *6*, 1157−1164.
(39) Medlycott, E. A.; Hanan, G. S. *Coord. Chem. Rev.* **2006**, *250*, 1763−1782.
(40) Maestri, M.; Armaroli, N.; Balzani, V.; Constable, E. C.; Cargill, Thompson, A. M. W. *Inorg. Chem.* **1995**, *34*, 2579−2767.
(41) Duati, M.; Tasca, S.; Lynch, F. C.; Bohlen, H.; Vos, J. G.; Stagni, S.; Ward, M. D. *Inorg. Chem.* **2003**, *42*, 8377−8384.
(42) Barigelletti, F.; Ventura, B.; Collin, J. P.; Kayhanian, R.; Gavina, P.; Sauvage, J. P. *Eur. J. Inorg. Chem.* **2000**, 113−119.
(43) Harriman, A.; Mayeux, A.; De Nicola, A.; Ziessel, R. *Phys. Chem. Chem. Phys.* **2002**, *4*, 2229−2235.

Table 6. Parameters from Fits to Eq 2 for $[Ru(\mathbf{3})_2]^{2+}$ and $[Ru(\mathbf{4})_2]^{2+}$

complex	A_1 (s^{-1})	ΔE_1 (cm^{-1})	A_2 (s^{-1})	ΔE_2 (cm^{-1})	M (s^{-1})	C (K)	Tm (K)	k_0 (s^{-1})
$[Ru(\mathbf{3})_2]^{2+}$	8.5×10^5	230	6.9×10^9	1960	2.6×10^5	7170	113	2.4×10^5
$[Ru(\mathbf{4})_2]^{2+}$	7.2×10^5	135	9.2×10^{10}	2200	2.4×10^6	2610	128	8.4×10^5
$[Ru(bpy)_3]^{2+}$ [a]	2.4×10^6	200	1.3×10^{14}	4000	[c]	[c]	[c]	[c]
$[Ru(tpy)_2]^{2+}$ [b]	2.1×10^7	560	1.7×10^{13}	1700	[c]	[c]	[c]	9.5×10^4

[a] From Macatangay et el. *Inorg. Chem.* **1996**, *35*, 6823. [b] From ref 43. [c] No data given.

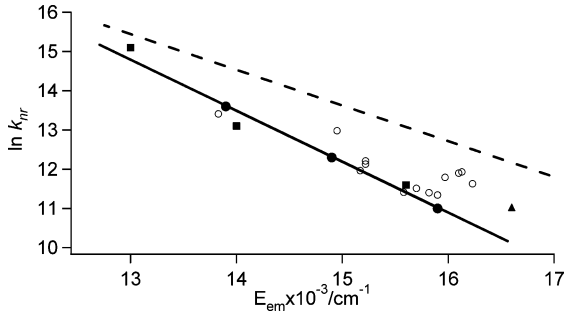

Figure 6. Energy gap law plot with the rate constant for nonactivated, nonradiative excited-state decay for the series $[Ru(\mathbf{4})_2]^{2+}$, $[Ru(\mathbf{3})_2]^{2+}$, $[Ru(ttpy)_2]^{2+}$, $Ru(tpy)_2]^{2+}$ versus emission energy (data from Table 4, ref 21 and Norrby, T. et al. Inorg. Chem., **1997**, 36, 5850. Filled circles = 80 K, filled squares = 130−150 K (above the glass transition temperature of the solvent), triangle = data for $[Ru(tpy)_2]^{2+}$. The solid line is a linear fit to the data (triangle excluded). The dashed line represents the energy gap law behavior reported for bipyridine and bipyrazine complexes in ref 33. Open circles correspond to data for various substituted Ru−bisterpyridine complexes as reported by Maestri et al. in ref 37.

and it indeed displays a similar, less-remarkable, excited-state lifetime (180 ns) as other bis-tridentate ruthenium complexes with an emission maximum close to 800 nm.

(ii) Effect of Emission Energy on k_{nr}. For the second question above, although a decrease in MLCT energy may reduce the activated decay via MC states, the direct nonradiative decay to the ground state might instead increase, according to the energy gap law.[26−29] In Figure 6, we plot the rate of nonradiative decay just above and below the glass transition region against the emission energy (at the wavelength maximum) for $[Ru(\mathbf{3})_2]^{2+}$, $[Ru(\mathbf{4})_2]^{2+}$, $[Ru(ttpy)_2]^{2+}$, and $[Ru(tpy)_2]^{2+}$. With the exception of $[Ru(tpy)_2]^{2+}$, the data seem to follow a typical exponential energy gap law. The correlation also agrees well with the (somewhat scattered) data for substituted Ru−bisterpyridines reported by Maestri et al.[40] For comparison, a dotted line representing the data for Ru−bipyridine complexes[33] is included. It is clear that the tridentate complexes show a slower decay than the bidentate ones at a corresponding energy. This may be explained by their smaller Huang−Rhys parameter (S_M = 0.5−0.7) compared to the tris-bidentate complexes ($S_M \approx$ 0.95, typically),[33] corresponding to a smaller excited-state distortion, as the excess electron is delocalized over a larger conjugated system in the MLCT state. This smaller distortion in turn reduces the Franck−Condon overlap for the nonradiative decay. The steeper slope in Figure 6 for the tridentate complexes is consistent with the energy gap law, as the slope is predicted to be inversely related to the magnitude of the Huang−Rhys parameter:[19,26,28]

$$\ln k_{nr} \propto [(\ln(E_{00}/\hbar\omega_M S_M) - 1)/\hbar\omega_M]E_{00} \qquad (3)$$

The values of the slope, which are −1300 and −900 cm for the tridentate and bidentate complexes, respectively, are in good agreement with the prediction of eq 3 using the values of S_M given above and $\hbar\omega_M \approx 1300$ cm^{-1}. The data points in Figure 6 are too few to prove the validity of the energy gap law for this series ($[Ru(\mathbf{4})_2]^{2+}$, $[Ru(\mathbf{3})_2]^{2+}$, $[Ru(ttpy)_2]^{2+}$, and $Ru(tpy)_2]^{2+}$) of bis-tridentate complexes. They are clearly consistent with eq 3, however, so that the value of k_{nr} seems to be governed by the emission energy, with no obvious difference between five- and six-membered chelate rings in bis-tridentate complexes. Furthermore, Figure 6 implies that the emissive excited state is similar in nature for all of the bis-tridentate complexes included in this study and so supports the conclusion from above that the emissive state is of MLCT character also in $[Ru(\mathbf{4})_2]^{2+}$.

(iii) The Nature of the Higher State. The nature of the higher state responsible for the activated process discussed above can be deduced from the frequency factors in eq 2. The frequency factor, A_2 lies in the range $10^{12}-10^{14}$ s^{-1}, for almost all of the tris-bidentate and bis-tridentate Ru(II) complexes reported in the literature, as is expected for an irreversible surface crossing between ^{3}MLCT and ^{3}MC states. In contrast, for the complexes studied here, the frequency factor A_2 is much lower: $A_2 = 10^9-10^{10}$ s^{-1} (Table 6). In a few cases, A_2 values on the order of 10^7-10^8 s^{-1} have been observed. The latter behavior is usually interpreted as representing a population of a higher MLCT state, in the few cases where deactivation to MC states is less significant, and the presence of a fourth MLCT state can be distinguished.[33−38] Instead, we know of only two cases when frequency factors and activation energies in the range observed here have been reported for ruthenium complexes: for $[Ru(bpy)_2(CN)_2]$[36] and $[Ru(bpy)(bpyz)_2]^{2+}$ (bpyz = bipyrazine)[33]. The explanation offered has been that the reverse surface crossing MC to MLCT would be much faster than the deactivation of the MC state by other routes, so that a pre-equilibrium is set up. In such a case, the observed activation energy would be the free-energy difference between the MLCT and MC states, and the frequency factor would be the decay rate constant of the MC state via the other route(s).

Frequency factors in the range 10^9-10^{10} s^{-1} must not necessarily imply that the higher state is an MC state, however. For $[Ru(\mathbf{4})_2]^{2+}$, the activation energy $\Delta E_2 = 2200$ cm^{-1} and the MLCT energy is ca. 3000 cm^{-1} lower than that in the parent $[Ru(tpy)_2]^{2+}$. The ligand structure and expected coordination geometry is very similar between these complexes. Moreover, the complexes $[Ru(bpy)_3]^{2+}$, $[Ru(phen)_3]^{2+}$, and $[Ru(bpy)_2(iso\text{-}biq)]^{2+}$ all have very similar emission energies, $Ru^{3+/2+}$ potentials, and activation energy ΔE_2,[15,31,33,36] and these ligands should therefore give similarly strong ligand fields. Therefore, if ligand **4** can be viewed as

a combination of a phen and "half an iso-biq", one would expect a ligand field-splitting capacity similar to that for tpy. Consequently, if the MC state in $[Ru(\mathbf{4})_2]^{2+}$ would be only 2200 cm^{-1} above the lowest MLCT state, then the MLCT and MC states in $[Ru(tpy)_2]^{2+}$ would be below the MLCT state. Although we cannot exclude this situation, it seems more probable that the higher state observed for $[Ru(\mathbf{3})_2]^{2+}$ and $[Ru(\mathbf{4})_2]^{2+}$ is instead a higher MLCT state.

It has also been suggested that preexponential factors in the range observed for $[Ru(\mathbf{3})_2]^{2+}$ and $[Ru(\mathbf{4})_2]^{2+}$ can be due to a combination of activated decay via both MC and MLCT states.[44] However, incorporation of another Arrhenius term into eq 2 does neither lead to significantly better fits or to parameters that clearly indicate surface crossing to MC and MLCT states, respectively. Therefore, we prefer our interpretation above, which is that a higher MLCT state is responsible for the second Arrhenius term in the deactivation.

The higher-energy state in the present complexes has a higher intrinsic nonradiative decay rate than the lower-energy MLCT states, leading to a decrease in emission quantum yield at higher temperature: Whereas k_r is about the same above and below the glass transition temperature (150 and 80 K, respectively) in both $[Ru(\mathbf{3})_2]^{2+}$ and $[Ru(\mathbf{4})_2]^{2+}$, it decreases significantly at 298 K. The relative energies of MLCT states, and the intrinsic properties of a fourth MLCT state, will depend on the ligands involved. The higher values of ΔE_2 and A_2, the latter being equal to the inverse lifetime of the upper state, compared to previous reports of a fourth MLCT state in Ru−bipyridines,[33−36] should therefore not be surprising.

(iv) The Bis-Tridentate Complexes. Finally, we discuss the results for $[Ru(bpy)_2(\mathbf{1})]^{2+}$ and $[Ru(bpy)_2(\mathbf{2})]^{2+}$. The effect on the emission lifetime of introducing a quinoline-based six-membered chelate ring in the tris-bidentate complexes is opposite to that in the bis-tridentate complexes. The room-temperature emission lifetime and energy of $[Ru(bpy)_2(\mathbf{2})]^{2+}$ are very similar to the case of $[Ru(bpy)_2(biq)]^{2+}$, and the slight decrease in lifetime compared to that of $[Ru(bpy)_3]^{2+}$ can probably be ascribed to the lower emission energy, following the energy gap law. Although the electronic difference between the coordinated, isomeric ligands **1** and **2** are also significant, one possible explanation for the much-shorter lifetime of $[Ru(bpy)_2(\mathbf{2})]^{2+}$ is that the octahedral character is already rather good in the parent $[Ru(bpy)_3]^{2+}$ complex. Introduction of **1** gives a somewhat distorted structure, with elongated Ru−N bonds (crystallographic results) and a steric interaction with the neighboring bpy ligands that rather increases deactivation via MC states. This effect has been established for 6-substituted bpy complexes.[16,23,41,45−47] The low-temperature spectra for such distorted complexes show a poorly resolved vibrational structure,[23] meaning that the ground-MLCT-state geometric distortion is unusually large, especially in the low-frequency modes (Ru−N vibrations). Elongation of the Ru−N bonds will make the MLCT geometry more similar to the MC states and increase the rate of surface crossing, resulting in short excited-state lifetimes. It is reasonable that bidentate complexes are more sensitive to these sterically induced distortions than tridentate ones, and this reasoning is supported by the fact that the emission spectra for the latter show a better-resolved vibrational structure (Figure 4).

Concerning the effect of an in-plane distortion as compared to a dihedral one (Introduction), we note that the electronic properties do in fact change significantly with an in-plane distortion in $[Ru(bpy)_2(\mathbf{1})]^{2+}$. Although the electrochemical potentials for the first reduction and oxidation are shifted by only 0.05−0.1 V compared to the values for $[Ru(bpy)_3]^{2+}$, and the MLCT absorption maximum is similar, the ^{3}MLCT energy is reduced by about 0.25 eV. Also, the electrochemical potentials are very different compared to the isomeric $[Ru(bpy)_2(\mathbf{2})]^{2+}$. An even more-substantial difference between the complexes is seen in the room-temperature excited-state lifetime, as already discussed.

Conclusions

In conclusion, the deactivation via MC states in $[Ru(\mathbf{3})_2]^{2+}$ and $[Ru(\mathbf{4})_2]^{2+}$ is slowed down substantially compared to the parent complex $[Ru(tpy)_2]^{2+}$, leading to much-longer excited-state lifetimes. The effect cannot be explained only by the decrease in the MLCT energy. We suggest that the activated process seen at higher temperatures is not due to MC states but to a higher MLCT state. There is no simple and general effect of the number of atoms in the chelate ring on the photophysical properties of ruthenium complexes. A larger chelate ring increases the room-temperature excited-state lifetime of the bis-tridentate complexes studied, whereas the effect is the opposite for tris-bidentate compounds. The long ^{3}MLCT lifetime of $[Ru(\mathbf{3})_2]^{2+}$ is probably due to a larger bite angle, giving a more-octahedral complex and thus an increased ligand field strength and a reduced rate of deactivation via MC states. The short excited-state lifetime of $[Ru(bpy)_2(\mathbf{1})]^{2+}$ can probably be attributed to the larger sensitivity of tris-bidentate complexes to steric repulsion, an explanation supported by the shape of the emission spectra. Nevertheless, the result for $[Ru(\mathbf{3})_2]^{2+}$ is encouraging in that it shows an unusually long room-temperature MLCT lifetime of 810 ns and that the incorporation of a six-membered chelate ring is a viable way of improving the photophysical properties of bis-tridentate Ru−polypyridine complexes.[2,4]

Experimental Section

Nuclear Magnetic Resonance. Spectra were recorded on a General Electric QE-300 Spectrometer at 300 MHz and referenced to the solvent peak in CD_3CN. A household microwave oven (Samsung, MW 2000 U, 950 W, 60 Hz) was modified according to a previously published description.[48,49] Elemental analyses were performed by Quantitative Technologies, Inc., P.O. Box 470,

(44) Sykora, M.; Kincaid, J. R. *Inorg. Chem.* **1995**, *34*, 5852−5856.
(45) Bardwell, D. A.; Barigelletti, F.; Cleary, R. L.; Flamigni, L.; Guardigli, M.; Jeffery, J. C.; Ward, M. D. *Inorg. Chem.* **1995**, *34*, 2438−2446.
(46) Fabian, R. H.; Klassen, D. M.; Sonntag, R. W. *Inorg. Chem.* **1980**, *19*, 1977−1982.
(47) Kelly, J. M.; Long, C.; O'Connell, C. M.; Vos, J. G.; A., T. A. H. *Inorg. Chem.* **1983**, *22*, 2818−2824.
(48) Matsumura-Inoue, T.; Tanabe, M.; Minami, T.; Ohashi, T. *Chem. Lett.* **1994**, 2443.
(49) Arai, T.; Matsumura, T.; Oka, T. *Kagaku to Kyoiku* **1993**, *41*, 278.

Whitehouse, NJ 08888. Literature procedures were followed for the preparation of 8-(pyrid-2′-yl)quinoline (**1**),[6] 8-(1′,10′-phenanthroline-2′-yl)quinoline (**3**),[7] [Ru(**2**)(bpy)$_2$](PF$_6$)$_2$,[9] [Ru(**4**)$_2$](PF$_6$)$_2$,[8] [Ru(bpy)$_2$Cl$_2$]·2H$_2$O,[50] and [Ru(tpy)Cl$_3$]·3H$_2$O.[51]

[Ru(1)(bpy)$_2$](PF$_6$)$_2$ A mixture of 8-(pyrid-2′-yl)quinoline (**1**, 0.05 g, 0.25 mmol) and [Ru(bpy)$_2$Cl$_2$]·2H$_2$O in 3:1 EtOH/H$_2$O (5 mL) was heated under reflux for 4 h. To the cooled solution was added NH_4PF_6 (85 mg, 0.52 mmol), and the solution was stirred for 0.5 h. The EtOH was partially evaporated, and the resulting precipitate was collected and washed with H$_2$O (3 × 15 mL), Et$_2$O (3 × 20 mL), and dried to afford the complex as a red solid (0.21 g, 86%): ^{1}H NMR (CD_3CN) showed a complex set of 26 overlapping signals 8.7−7.1 ppm. The complex [Ru(**1**)(bpy-d$_8$)$_2$](PF$_6$)$_2$ was prepared from **1** and [Ru(bpy-d$_8$)$_2$Cl$_2$] in an analogous manner and showed only 10 peaks in its ^{1}H NMR (CD_3CN): δ 8.41 (d, 1H, H_7), 8.31 (overlapping t, 2H, $H_{3'}$ and $H_{4'}$), 8.08 (d, 1H, H_5), 7.97 (overlapping d, 2H, H_2 and $H_{6'}$), 7.78 (t, 1H, H_6), 7.47 (t, 1H, H_4), 7.15 (dd, 1H, $H_{5'}$), 7.09 (dd, 1H, H_3). These same 10 peaks were all found in the NMR of the undeuterated sample. An X-ray quality crystal of the protio complex was grown by the diffusion of benzene into a CH_3CN solution.

[Ru(3)$_2$](PF$_6$)$_2$. A mixture of 8-(1′,10′-phenanthrolin-2′-yl)-quinoline (**3**, 61.4 mg, 0.2 mmol) and $RuCl_3$·3H$_2$0 (26.1 mg, 0.1 mmol) in ethylene glycol (15 mL) was heated in a microwave oven for 15 min. The mixture was cooled to 25 °C, and NH_4PF_6 (65.2 mg, 0.4 mmol) in H$_2$O (100 mL) was added. The solution was stirred for 20 min, and the red precipitate was filtered, dried, and chromatographed on Al_2O_3 (30 g), eluting with CH_3CN/toluene (1:1) to afford [Ru(**3**) $_2$](PF$_6$)$_2$ as a red solid (36 mg, 36%), mp >270 °C: ^{1}H NMR (CD_3CN) δ 9.13 (AB quartet, 4H, $H_{5',6'}$), 9.05 (dd, 2H, H_7, J = 7.5 Hz), 8.40 (d, 2H, $H_{3'}$ or $_{4'}$, J = 8.7 Hz), 8.30 (dd, 2H, H_4, J = 7.2, 0.9 Hz), 8.18−8.10 (m, 8H, H $H_{3'}$ or $_4$ and H $H_{9',7',5}$), 7.99 (t, 2H, H H_6, J = 7.8 Hz), 7.46 (d, 2H, H_2, J = 5.4 Hz), 7.23 (dd, 2H, H_3, J = 8.1, 5.4 Hz), 6.86 (dd, 2H, $H_{8'}$, J = 8.1, 5.4 Hz); Anal. Calcd for $C_{42}H_{26}N_6RuP_2F_{12}$·H$_2$O: C, 49.27; H, 2.74; N, 8.21. Found: C, 49.38; H, 2.39; N, 8.15.

X-ray Determination of [Ru(1)(bpy)$_2$](PF$_6$)$_2$. All of the measurements were made with a Siemens SMART platform diffractometer equipped with a 1K CCD area detector. A hemisphere of data (1271 frames at 5 cm detector distance) was collected using a narrow-frame method with scan widths of 0.30° in omega and an exposure time of 25 s/frame. The first 50 frames were remeasured at the end of the data collection to monitor instrument and crystal stability, and the maximum correction on I was <1%. The data were integrated using the Siemens *SAINT* program, with the intensities corrected for the Lorentz factor, polarization, air absorption, and absorption due to variation in the path length through the detector faceplate. A psi scan absorption correction was applied based on the entire data set. Redundant reflections were averaged. Final cell constants were refined using 6517 reflections having $I > 10\sigma(I)$, and these, along with other information pertinent to data collection and refinement, are listed in Table 2. The Laue symmetry was determined to be 2/*m*, and from the systematic absences noted the space group was shown unambiguously to be *P*2(1)/*c*. One of the anions was found to be disordered over three different orientations, and this was treated by the use of ideal rigid bodies having occupancy factors of 45, 35, and 20%.

UV−Vis Absorption. Spectra were recorded on a Varian Cary 50 UV−vis instrument or on a Hewlett-Packard 8453 diode array instrument.

Cyclic Voltammetry. CV was carried out in a three-compartment cell connected to an Autolab potentiostat with a GPES electrochemical interface (Eco Chemie). A glassy carbon disc (diameter 3 mm, freshly polished) was used as the working electrode. The potentials were measured versus a nonaqueous Ag/Ag^+ reference electrode (CH Instruments, 10 mM $AgNO_3$ in acetonitrile) with the ferrocenium/ferrocene ($Fc^{+/0}$) couple in acetonitrile as an internal standard. Solutions were prepared from dry acetonitrile (Merck, spectroscopy grade, dried with MS 3 Å) and contained ca. 1 mM of the analyte and 0.1 M tetrabutylammonium hexafluorophosphate (Fluka, electrochemical grade, dried at 373 K) as the supporting electrolyte. Oxygen was removed by bubbling the stirred solutions with solvent-saturated argon, and the samples were kept under an argon atmosphere during measurements.

Transient Absorption. Measurements were performed with a frequency-tripled Q-switched Nd:YAG laser from Quantel, producing <10 ns flashes. Excitation light at different wavelengths was obtained in an optical parametric oscillator. The analyzing light was obtained from a 150 W xenon lamp. The emission was detected at a right angle with a monochromator and a P928-type PMT. The PMT output was recorded on a Hewlett-Packard digital oscilloscope (2 G samples/s). The measurements were performed in 1 × 1 cm quartz cuvettes in acetonitrile of spectrophotometric grade, and samples were bubbled with argon to remove oxygen. Femtosecond transient absorption spectra were recorded using a system previously described.[52] Briefly, the output from a TOPAS OPA (100 fs, 400−800 nJ) was used as pump pulses and overlapped in the sample with white-light continuum probe pulses generated from 100 fs 800 nm pulses in a CaF_2 plate. Residual 800 nm light was removed with a KG3 glass filter. The sample (OD < 0.2 at the pump wavelength) was contained in a 1 mm quartz cell, which was continuously moved to avoid bleached spots and accumulation of photoproducts.

Steady-State Emission. Measurements were performed on a SPEX-Fluorolog II fluorimeter or on a SPEX Fluorolog-3 and corrected for different detector sensitivity at different wavelengths. Low-temperature measurements were performed in a variable temperature liquid nitrogen cryostat from Oxford Instruments, and the temperature was set with either a temperature controller ITC601 or ITC502 from Oxford Instruments. All of the emission measurements were performed in 1 × 1 cm^2 quartz cuvettes. A 1:4 (v/v) MeOH−EtOH mixture was used as solvent at all temperatures.

Time-Resolved Emission. Measurements for the long-lived complexes were performed with a frequency-tripled Q-switched Nd:YAG laser from Quantel, producing <10 ns flashes. Excitation light at different wavelengths were obtained in an optical parametric oscillator. The emission was detected at a right angle with a monochromator and a P928-type PMT. The PMT output was recorded on a Hewlett-Packard digital oscilloscope (2 G samples/s). For the less-long-lived complex, a time-correlated single photon counting setup was used. Excitation light was produced with a Coherent Verdi V18 diode pump laser in a regenerative amplified system. The wavelength used for excitation was 400 nm. The emission was detected at a magic angle and perpendicular to the excitation light. Blue filters were used to remove the remains of 800 nm light in the excitation beam, and red filters were used to remove scattered light in the detection. The emitted light was

(50) Sullivan, B. P.; Salmon, C. J.; Meyer, T. J. *Inorg. Chem.* **1978**, *17*, 3334.
(51) Sullivan, B. P.; Calvert, J. M.; Meyer, T. J. *Inorg. Chem.* **1980**, *19*, 1404−1407.
(52) Andersson, M.; Davidsson, J.; Hammarstrom, L.; Korppi-Tommola, J.; Peltola, T. *J. Phys. Chem. B* **1999**, *103*, 3258−3262.

collected by an MCP photomultiplier. Oxygen-free samples for temperature-dependent measurements were prepared using a freeze−pump−thaw method, and the cuvettes were sealed throughout the measurements.

Acknowledgment. M.A., H.C.B., and L.H. thank the Swedish Energy Agency and the Knut and Alice Wallenberg Foundation for generous financial support. C.B., C.C., and R.T. thank the Robert A. Welch Foundation (E-621) and the National Science Foundation (CHE-0352617) for generous financial support. We also thank Dr. James Korp for assistance with the X-ray crystallography.

Supporting Information Available: X-ray crystallographic files for [Ru(**1**)$(bpy)_2$]$(PF_6)_2$ (in CIF format). This material is available free of charge via the Internet at http://pubs.acs.org.

IC7011827